



Modeling and optimization of cationic dye adsorption onto modified SBA-15 by application of response surface methodology

Zeinab Salahshoor, Afsaneh Shahbazi*

Environmental Sciences Research Institute, Shahid Beheshti University, G.C., Tehran 1983969411, Iran, emails: zsalahshoor@yahoo.com (Z. Salahshoor), a_shahbazi@sbu.ac.ir (A. Shahbazi)

Received 18 January 2015; Accepted 3 June 2015

ABSTRACT

SBA-15 mesoporous silica was modified with melamine-based dendrimer amine (MDA) via grafting approach and used as adsorbent for the removal of methylene blue (MB) cationic dye from aqueous solution. The synthesized material, denoted MDA-SBA-15, was characterized by means of X-ray diffraction, Fourier transform infrared spectroscopy, scanning electron microscopy, and N₂ adsorption–desorption, in order to prove the 2D hexagonal mesoporous structure and covalent grafting of MDA onto SBA-15. Central composite design combined with response surface methodology (RSM) was employed for statistical modeling, optimization, and analysis the effects of influence variables such as the initial pH (3–10), adsorbent doses (0.5–3.5 g L⁻¹), temperature (25–40°C), and initial concentrations (10–30 mg L⁻¹) onto the MB removal. From the analysis of variance, pH and temperature were identified as the most influential factors onto each experimental design response. Maximum percentage removal (98%) under optimum conditions of variables (pH of 10, adsorbent dose of 3 g L⁻¹, MB concentration of 10 mg L⁻¹, and temperature of 25°C), as predicted by RSM, was found to be very close to the experimentally determined value (95.5%). The Langmuir, Freundlich, and Temkin isotherm models were used to describe the equilibrium sorption of MB by MDA-SBA-15, and the Langmuir isotherm showed the best concordance as an equilibrium model. The obtained kinetic data manifested that adsorption kinetics was more accurately exposed by a pseudo-second-order model and film diffusion was the rate-determining step for the adsorption of MB onto MDA-SBA-15. The associated thermodynamic parameters reveal that the process of adsorption is spontaneous and exothermic nature within the studied temperature range.

Keywords: Adsorption; Cationic dye; SBA-15; Response surface methodology

1. Introduction

Humankind faces a serious problem with water contaminated by synthetic dyes since significant increase in the use of a wide variety of dyes and dyed products. Substantial quantities of water are

commonly used by major dye-consuming industries such as textile, leather goods, cosmetics, food, plastics, and consumer electronics resulting in generating huge volume of toxic wastewater contaminated with highly colored synthetic dyes that are drained to local water resources (10–35% dye is lost in the effluent during the dyeing process in textile industry) [1,2]. The presence of dyes in aquatic bodies increases chemical

*Corresponding author.

oxygen demand, color contents, dissolved and suspended solids, impedes light penetration into water, interfere photosynthesis of aquatic plants, hinders the growth of microbes, creates microtoxicity to fish and other organisms, etc. Above all, the carcinogenic and mutagenic nature of the dyes is detrimental to human beings [3]. Among classes of dyes, the cationic dyes are commonly used for different purposes due to their ease of applicability, durability, and good fastness to materials. Methylene blue (MB) is the most commonly cationic dye that used for dyeing cotton, wood, and silk. It can cause permanent injury to the human eyes and gives rise to respiratory problem, while oral ingestion produces a burning sensation and may cause nausea, vomiting, profuse sweating, mental confusion, and methemoglobinemia [3–5]. There are various techniques that used for the remediation of dye wastewater such as oxidation, ozonation, coagulation and flocculation, membrane separation, and adsorption. Adsorption using a variety of sorbents is preferable because of its reusability, cost-effectiveness, and easy to operate [3,6,7]. In the case of adsorption techniques, great effort has been directed toward the adsorption of dye using mesoporous silica adsorbents because of their high surface area, surface reactivity, structural stability, and regular channel-type structures [8–10]. Among these mesoporous silica, SBA-15 is the most popular because of its large, adjustable pores (5–30 nm), which allow easier accessibility of target species to the inner surface of the material, leading to fast kinetics of chemical or physical processes, and also because of its thick pore walls, around 4 nm, which provide enhanced mechanical stability [11–13]. In addition, SBA-15-based adsorbents can remove a wide variety of toxic pollutants with high efficiency by modification with appropriate ligands. The dendrimer amine-functionalized mesoporous silicas have been particularly explored for the water remediation purposes. When dendrimer is terminated with amine ligands, not only do the lone pair electrons bind, but also may cooperatively enhance activity and selectivity [6]. Melamine-based dendrimer amines (MDAs) are such ideal dendrimer ligands due to intensively binding amine sites and also to their enhanced hydrophilic silica surface compared to analogous adsorbents [14]. Various physical and covalent strategies have been developed to achieve amine-functionalized mesoporous silicas. For this aim, grafting approach has been considered as an alternate route. In spite of partial success in the treatment of dyes using the SBA-15, no studies for adsorption of MB by MDA-SBA-15 has been found. In this work, adsorption behavior of MDA-SBA-15 was evaluated against MB cationic dye. During the adsorption process, there are several main

factors that affect the adsorption efficiency. Generally, the conventional optimization process is studied by varying one factor while maintaining other factors fixed. A statistical optimization method can overcome the limitations of the conventional method and proves to be a useful method for process optimization. Response surface methodology (RSM) is a collection of mathematical and statistical techniques for designing experiments, building models, and analyzing the interactive effects of independent factors. In particular, the main advantage of the response surface approach lies in the fact that it can optimize a process with a reduced number of planned experiments. From an economic point of view, a response surface approach coupled with central composite design (CCD) is adequate to optimize the adsorption process and assess the effects of the operating parameters initial concentration, pH, temperature, and adsorbent dose, for the adsorption efficiency onto the MDA-SBA-15 from dye solution. The results provide a mathematical model for optimizing the adsorption process and demonstrate the efficiency of the SBA-15 adsorbent modified with dendrimer amine. Also the mechanistic nature of the adsorption process was estimated by applying the isotherm models. In addition, the thermodynamics and kinetic parameters associated with the adsorption process were also evaluated.

2. Materials and methods

2.1. Chemicals and reagents

Tetraethylorthosilicate (TEOS) used as the silica source for SBA-15 was supplied by Aldrich. Triblock poly (ethylene oxide)-*b*-poly (propylene oxide)-*b*-poly (ethylene oxide) copolymer Pluronic P123 (MW = 5,800) purchased from Aldrich was used as structure directing agent. The functionalization agent, obtained from Aldrich was 3-aminopropyltrimethoxy-silane, herein referred to as APTS. *N,N*-di-isopropylethylamine (DIPEA), 2,4,6-trichloro-1,3,5-triazine (cyanuric chloride), ethylenediamine (EDA), tetrahydrofuran, hydrochloric acid (HCl, 37%), toluene, and methanol were provided from Merck. The dye, MB (molecular formula = $C_{16}H_{18}N_3SCl$, $\lambda_{max} = 663$ nm, MW = 319.85 g mol⁻¹), was obtained from Aldrich. In addition, all solutions were prepared under the protection of N₂ and used right after they were ready.

2.2. MDA-SBA-15 synthesis

The SBA-15 was prepared in aqueous hydrochloric acid using dilute solutions of the non-ionic block copolymer surfactant Pluronic P123 following the

literature [15]. Briefly, 4 g of Pluronic P123 was dissolved in 90 ml of 2 M HCl solution and 21 ml distilled water at 25°C. Then 6.4 g of TEOS was added. After stirring at 40°C for 24 h, the solution was transferred to a Teflon-lined autoclave which was kept at 100°C for 24 h. The resulting material was recovered by filtration and washed with deionized water several times. The organic template (Pluronic P123) was removed by calcination at 550°C for 6 h under air. The material was then filtered and dried under vacuum. The grafting of amine on SBA-15 was achieved using a precursor of 3-aminopropyl-trimethoxysilane. A mixture of 5 g of calcined SBA-15 with 50 ml of toluene and 7 ml of 3-aminopropyltrimethoxysilane was stirred and refluxed 24 h. The resulting 3-aminopropyl-grafted SBA-15 was washed repeatedly with dried toluene and then dried under a vacuum at 80°C overnight. It will be denoted as APTS-SBA-15 (NH₂-SBA-15). APTS-SBA-15 functionalized by melamine-based dendrimer amine was prepared using similar method to that reported in the literature [14]. Cyanuric chloride (5.5 g, 30 mmol) and diisopropylethylamine (7.1 ml) were dissolved in tetrahydrofuran (300 ml) in a round bottom flask. This mixture was stirred at 0°C. APTS-SBA-15 was added with continuous stirring to the above mixture. After that the mixture was left to react at 0°C for 20 h. Afterwards the solid was filtered and washed twice with 80 ml of methanol, 80 ml dichloromethane and 80 ml tetrahydrofuran. The washed solid was then collected and added to a mixture of ethylenediamine (4 ml, 73.84 mmol) and THF (300 ml). After completing the addition the mixture is then refluxed for 24 h at 65–70°C. The solid was collected by filtration then washed as previously described. This solid is referred to as MDA-SBA-15.

2.3. Characterization

The SBA-15, NH₂-SBA-15, and MDA-SBA-15 were structurally characterized by powder X-ray diffraction in a Philips X'pert, Netherlands equipped with a liquid nitrogen-cooled germanium solid-state detector using Cu K α radiation over the range of 0.8°–10° 2 θ . The morphology of the mesoporous materials was obtained by scanning electron microscopy (SEM) on a LEO 1455 VP electron microscope. The textural properties of the samples were determined by nitrogen adsorption-desorption isotherms at –196°C using a BELsorp-mini II, Japan. Prior to each analysis, the samples 0.1 g was degassed under vacuum at 100°C for 3 h. The surface area was determined by the BET method, whereas the pore size distribution was calculated using the Barrett-Joyner-Halenda (BJH) approach. The Fourier transform infrared spectra (FT-IR) were recorded with

in a 400–4,000 cm^{–1} region on a Bruker Vector 22 infrared spectrophotometer, Japan.

2.4. Adsorption studies

Batch adsorption studies were performed by suspending MDA-SBA-15 (0.5–3.5 g L^{–1}) in MB solution of different initial concentrations (10–30 mg L^{–1}) having various initial pH values (3–10). The suspensions were continuously agitated (250 rpm) at constant temperature (25–40°C), and aliquots were drawn at regular intervals of time until equilibrium was reached. At the end of the adsorption period, the supernatant solutions were centrifuged and the concentration of MB in the supernatant solution before and after the adsorption was determined using a calibration curve obtained by employing a UV/vis spectrophotometer at λ_{max} of 663 nm. The percentage removal ($R\%$) and adsorption capacity (q_e , mg g^{–1}) of MB by MDA-SBA-15 was calculated as follows:

$$R\% = \left(\frac{C_0 - C_e}{C_0} \right) \times 100 \quad (1)$$

$$q_e = \frac{(C_0 - C_e)V}{W} \quad (2)$$

where C_0 is the initial and C_e the equilibrium dye concentration (mg L^{–1}), W the adsorbent dose (g), and V the solution volume (L).

2.5. Experimental design and statistical analysis by RSM

RSM is an efficient statistical method that uses quantitative data of appropriate experiments for designing experiments, analyzing the relationships between the response and the independent variables, developing response surface models, and ultimately optimizing the process variables to achieve maximum response [16]. Four-factor, five-level central composite experimental design combining with response surface modeling and quadratic programming were applied to optimize the adsorption process of MB by MDA-SBA-15 and investigate the relative or interactive effects of solution pH, initial dye concentration, adsorbent dose, and temperature on the response ($R\%$).

In this study, a second-degree polynomial equation was approximated for the evaluating the effect of each independent variable on the response.

$$y = \beta_0 + \sum_{i=1}^k \beta_i X_i + \sum_{i=1}^k \beta_{ii} X_i^2 + \sum_{i=1}^k \sum_{j=1}^k \beta_{ij} X_i X_j + \varepsilon \quad (3)$$

where Y is the process response or output (dependent variable), k is the number of the patterns, i and j are the index numbers for pattern, β_0 is the free or offset term called intercept term, β_i the linear coefficients, β_{ii} the quadratic coefficients, β_{ij} the interaction coefficients, and X_i, X_j are the coded values of the independent process variables, and ε is the residual error.

In developing Eq. (3), the coded variables were obtained according to Eq. (4).

$$X = \frac{x - [x_{\max} + x_{\min}]/2}{[x_{\max} - x_{\min}]/2} \quad (4)$$

where x is the natural variable, X is the coded variable, and x_{\max} and x_{\min} are the maximum and minimum values of the natural variable. The experimental range and levels of independent variables considered in this study were presented in Table 1. The design matrix for four variables was varied at five levels ($-\alpha, -1, 0, +1, \alpha+$).

According to statistics theory, the four-factor, five-level CCD requires 27 sets of experiments, including 16 factorial points (2^n), 8 axial points ($2n$), and 3 replicates at the center point (n_c) as reported in Table 2.

2.6. Statistical analysis

In this study, the software Design-Expert 7.1.1 (State-Ease Inc.) was used to design the experiments and analyze the experimental data. Microsoft Excel[®] 2013 and SPSS were used for all calculations as data source running under Windows. The adequacy of the developed model and statistical significance of the regression coefficients were tested using the analysis of variance (ANOVA). An alpha (α) level of 0.05 was used to determine the statistical significance in all analyses. Results were assessed with various descriptive statistics such as p -value, F -value, degrees of freedom (df), determination coefficient (R^2), adjusted determination coefficient (R_a^2), sum of squares (SS),

mean sum of squares (MSS), coefficient of variation (CV), t -ratio, Mallow's C_p statistic, Durbin–Watson (DW) statistic, and chi-square (χ^2) test to reflect the statistical significance of the quadratic model [4,16]. The interaction among the different independent variables and their corresponding effect on the response was studied by analyzing the response surface 3D plots. For the validation of the regression model, a non-parametric Mann–Whitney (or Wilcoxon rank-sum) U -test and a two-sample (unpaired) t -test were performed to evaluate the relationship between the additional experimental data and the predicted responses. The measured and the model predicted values of the response variable (Y) were used to compute the correlation coefficient, the root mean square error of prediction (RMSEP), and the relative standard error of prediction (RSEP). The correlation between the measured and predicted values indicates the goodness of fit of the model, whereas the RMSEP and RSEP values are used to evaluate the predictive ability of the selected model [17,18]. The model equation was used to predict the optimum value and subsequently to elucidate the interaction between the factors within the specified range.

3. Result and discussions

3.1. Adsorbent characterization

The X-ray diffraction patterns, which were used to identify structural ordering of synthesized adsorbent, were presented in Fig. 1(a). As seen in Fig. 1(a), three resolved peaks were indexed as (1 0 0), (1 1 0), and (2 0 0) reflections associated with the hexagonal symmetry. Commonly found in materials like SBA-15, indicating a well-defined mesostructure. It was also pointed out that the peaks of NH₂-SBA-15 and MDA-SBA-15 shifted slightly to smaller angles as compared to SBA-15, which was attributed to the pore-filling effects that can reduce the scattering contrast between the pores and the silica walls and was already

Table 1
Experimental range and levels of independent variables

Variables	Notation	Range and levels			
		Low level (−1)	Center level (0)	High level (+1)	ΔX_i^a
Initial pH of solution	A	3	6.5	10	3.5
Initial concentration of dye (mg L ^{−1})	B	10	20	30	10
Adsorbent dose (g L ^{−1})	C	0.5	2.0	3.5	1.5
Temperature (°C)	D	25.0	32.5	40.0	12.5

^aStep change values.

Table 2
 CCD for four independent variables in coded and natural units

Batch no.	CCD term	Initial pH of solution (A)		Initial concentration of MB (B: mg L ⁻¹)		Adsorbent dose (C: g L ⁻¹)		Temperature (D: °C)		Observed responses	
		Uncoded	Coded	Uncoded	Coded	Uncoded	Coded	Uncoded	Coded	R (%)	q _e (mg g ⁻¹)
1	Center	6.5	0	20	0	2.0	0	32.5	0	58	5.8
2	Fact	3	-1	10	-1	3.5	1	25.0	-1	53	1.5
3	Fact	10	1	10	-1	3.5	1	40.0	1	66	1.8
4	Axial	6.5	0	20	0	2.0	0	28.8	-0.493	67	6.7
5	Axial	6.5	0	20	0	2.0	0	36.3	0.507	51	5.1
6	Fact	10	1	30	1	0.5	-1	40.0	1	52	31.7
7	Fact	3	-1	10	-1	0.5	-1	40.0	1	13	2.6
8	Axial	4.7	-0.5	20	0	2.0	0	32.5	0	50	5.0
9	Center	6.5	0	20	0	2.0	0	32.5	0	58	5.8
10	Center	6.5	0	20	0	2.0	0	32.5	0	58	5.8
11	Axial	6.5	0	15	-0.5	2.0	0	32.5	0	63	4.7
12	Fact	10	1	10	-1	3.5	1	25.0	-1	95	2.8
13	Axial	8.2	0.5	20	0	2.0	0	32.5	0	70	7.0
14	Axial	6.5	0	25	0.5	2.0	0	32.5	0	56	7.0
15	Fact	10	1	30	1	0.5	-1	25.0	-1	79	58.8
16	Fact	3	-1	30	1	3.5	1	40.0	1	17	1.4
17	Fact	3	-1	30	1	0.5	-1	40.0	1	4	2.4
18	Axial	6.5	0	20	0	1.25	-0.5	32.5	0	55	8.8
19	Fact	3	-1	10	-1	0.5	-1	25.0	-1	49	9.9
20	Fact	10	1	30	1	3.5	1	25.0	-1	94	8.1
21	Fact	3	-1	30	1	3.5	1	25.0	-1	43	3.7
22	Fact	3	-1	10	-1	3.5	1	40.0	1	21	0.6
23	Fact	3	-1	30	1	0.5	-1	25.0	-1	29	17.4
24	Fact	10	1	30	1	3.5	1	40.0	1	65	5.5
25	Fact	10	1	10	-1	0.5	-1	25.0	-1	89	17.8
26	Fact	10	1	10	-1	0.5	-1	40.0	1	55	11.0
27	Axial	6.5	0	20	0	2.75	0.5	32.5	0	64	4.6

observed in impregnation of mesoporous structures with organic compounds [14,19]. The morphology features of the SBA-15 were examined by SEM techniques. The typical SEM micrograph of SBA-15 sample was shown in Fig. 1(b). As could be seen, the SBA-15 silica displayed curved faceted and smooth rods based on elongated wheat-like macrostructures in SEM images with relatively uniform sizes of 1 μm [15,20].

The textural properties derived from BET surface area and BJH pore size distribution method were summarized in Table 3. The N₂ adsorption–desorption isotherm for all samples were depicted in Fig. 1(c). According to the IUPAC classification, all of the samples showed type of IV-shaped adsorption–desorption isotherm which is typical of mesoporous materials [14]. Moreover an H1 hysteresis loop is exhibited, which indicates that the SBA-15 structure is retained even after anchoring ligands. Grafting of MDA onto SBA-15 affected the BET specific surface area and

porosity of the hybrid, giving additional proof of the inner channel immobilization of functional groups [14,20]. The BET surface area declined from 604 to 293 m² g⁻¹ as the loading amount of functional groups onto SBA-15. The similar trend was observed for the total pore volume decreasing from 1.7 to 0.93 mL g⁻¹, concomitant with the mean pore diameters ranging from 7 to 4.7 nm.

The results of FT-IR showed that ligands were successfully grafted onto SBA-15 (Fig. 1(d)). In the case of non-functionalized SBA-15, very intense band at 1,088 cm⁻¹ corresponding to the Si–O stretching, and band at 462, 810 cm⁻¹ due to the Si–O–Si bending was observed. In mesoporous silica material this band could be assigned to the formation of the dense silica network [21]. The first functionalization step involved the grafting of aminopropyl on SBA-15 sample. The band at 1,635 cm⁻¹ was ascribed to NH₂ bending in NH₂-SBA-15 sample [14]. The characteristic peaks at 2,870 and 2,938 cm⁻¹ for the dendrimer functionalized

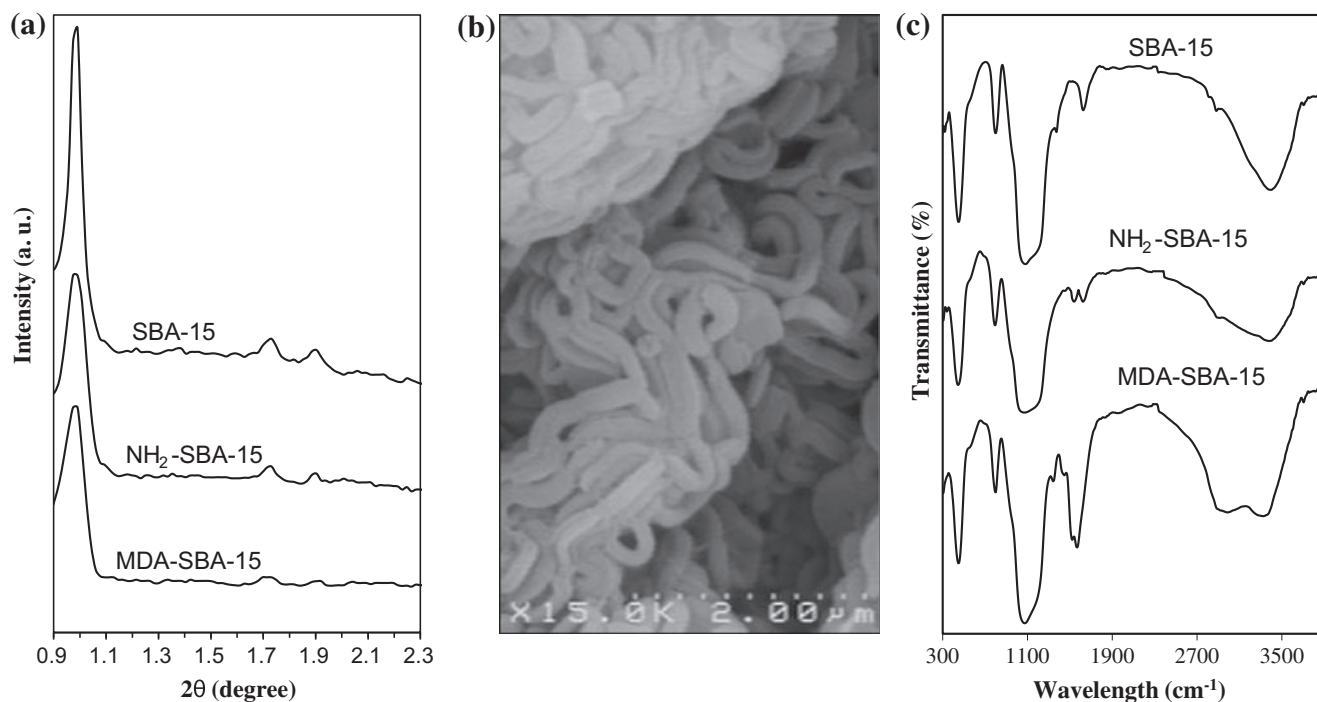


Fig. 1. (a) X-ray diffraction patterns, (b) scanning electron micrographs of SBA-15, (c) N_2 adsorption–desorption isotherm, and (d) Fourier transform infrared spectra of as synthesized SBA-15, NH_2 -SBA-15, and MDA-SBA-15 samples.

Table 3

Textural and structure parameters of SBA-15, NH_2 -Grafted SBA-15 and MDA-SBA-15. (D_{BJH} (nm): pore volume, S_{BET} ($m^2 g^{-1}$): BET specific surface area, V_{total} ($ml g^{-1}$): total pore volume)

Sample	D_{BJH} (nm)	S_{BET} ($m^2 g^{-1}$)	V_{total} ($ml g^{-1}$)
SBA-15	7.0	604	1.70
NH_2 -SBA-15	5.4	486	1.05
MDA-SBA-15	4.7	293	0.93

SBA-15 material could be ascribed to the C–H stretching vibration. Additionally, the bands at 1,434 and 1,573 cm^{-1} were attributed to the formation of aromatic triazine ring in MDA-SBA-15 [22]. These IR peaks were not found in the IR spectrum of the non-functionalized SBA-15 silica. Moreover, these bands revealed that SBA-15 has been successfully functionalized with NH_2 mono amine and MDA dendrimer amine.

3.2. Regression model development and statistical evaluation

CCD was used to define the relationships between response ($R\%$) and individual process variables.

Among linear, two-factor interaction (2FI), quadratic, and cubic polynomials, the quadratic model was considered to be most suitable for this process as it exhibited a lower standard deviation along with higher R^2 values and insignificant lack of fit (LOF). Following polynomial quadratic Eq. (5), which can be written in terms of coded parameters, was obtained performing regression modeling between response and coded values of four independent variables using the experimental data.

$$\begin{aligned}
 Y(R\%) = & 59.7 + 22.1X_A - 3.11X_B + 5.40X_C - 14.9X_D \\
 & + 2.34X_{AB} + 862X_{AC} + 0.0875X_{AD} + 1.24X_{BC} \\
 & - 0.763X_{CD} - 1.74X_A^2 - 3.74X_B^2 - 3.74X_C^2 \\
 & + 0.441X_D^2
 \end{aligned}
 \tag{5}$$

ANOVA was further carried out to justify the adequacy and significance of the models as given in Table 4. According to the results, F_{cal} value was higher than $F_{tab(n-df+1)}$ ($F_{cal} = 138 > F_{tab} = 2.64$), and p value was lower than 0.05, which showing the significance of the quadratic model and confirmed that the model was suitable for using in the current experiment. A plot of normal probability of the residuals was presented in Fig. 2, indicating almost no serious violation

Table 4
ANOVA of the quadratic model for adsorption of MB

Source	SS ^a	DF ^b	MSS ^c	F-Value	p-value	Remark
Model	13,700	14	978	138	<0.0001	Significant
A-pH	8,710	1	8,710	120	<0.0001	Significant
B-Conc.	253	1	253	23.8	<0.0001	Significant
C-Dose	492	1	492	71.9	<0.0001	Significant
D-Tem	3,750	1	3,750	545	<0.0001	Significant
AB	43.6	1	43.6	13.1	0.0044	Significant
AC	4.84	1	4.84	1.78	0.266	
AD	0.16	1	0.16	0.0183	0.836	
BC	32.5	1	32.5	3.66	0.0106	Significant
BD	50.4	1	50.4	7.01	0.00271	Significant
CD	0.49	1	0.49	1.39	0.717	
A ²	0.0113	1	0.0113	0.0749	0.956	
B ²	0.264	1	0.264	0.347	0.79	
C ²	0.85	1	0.85	0.347	0.634	
D ²	2.54	1	2.54	0.00483	0.415	

^aSum of squares.

^bDegrees of freedom.

^cMean sum of square.

of the assumptions underlying the analyses [23]. In addition, goodness of the model was double checked by the coefficient of determination (R^2) and the adjusted coefficient of determination (R^2_{Adj}). A fairly high R^2 and R^2_{Adj} value (0.994, 0.987 respectively) indicated that the experimental response values concord with the model predicted values and 99% of the variability in the response could be explained by the predicted model. Moreover, a closely high value of the adjusted correlation coefficient ($R^2 = 0.987$) also showed a high significance of the model. The R^2_{Adj} corrects the R^2 value for the sample size and the number of terms in the model. If there are many terms in the model and the sample size is not very large, the R^2_{Adj} may be noticeably smaller than the R^2 . In this study, the values of R^2_{Adj} and R^2 were found to be very close. A similar pattern has been reported by others for the second order RSM experiments based on CCD [7,16,18]. Furthermore, relatively lower value of coefficient of variation ($CV = 3.44\%$) indicates a better precision and reliability of the experiments carried out.

At the same time, the LOF is the variation of the data around the fitted model. LOF is a special investigative test for adequacy of a model fit, because the effects of the additional higher order terms are removed from the error. If the model does not fit the data well, this will be significant. P-value of LOF was zero indicted the model fit the response well [24]. Mallows's C_p statistic can be used to determine how many terms could be omitted from the response surface model. For a response surface model including all

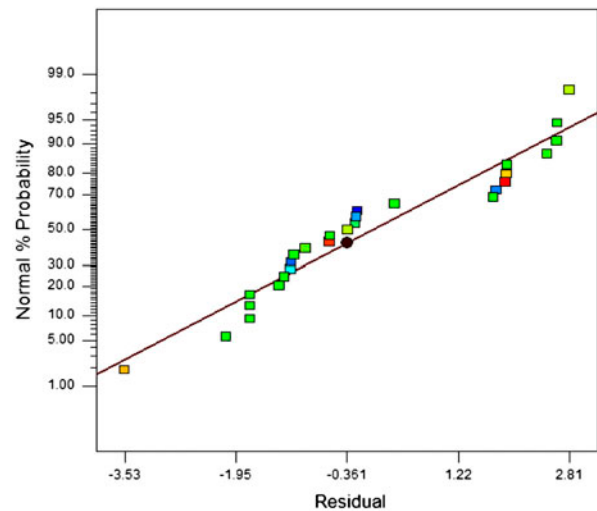


Fig. 2. The normal probability of the raw residuals.

terms, $C_p = p$, where p is the number of parameters or variables in the regression model including the intercept term. For response surface models with omitted terms, $C_p \sim p$ indicates a good model with little bias, and $C_p \leq p$ indicates a very good prediction model. The goal is to remove terms from the response surface model until a minimum C_p value near p is obtained. If $C_p > p$, this indicates that too many terms have been removed or some remaining terms are not necessary [25]. In this study, Mallows's C_p statistic ($C_p = 5$) indicated the third condition ($C_p \leq p, 5 \leq 15$), confirmed

that the model has a very good prediction. Auto-correlation or correlation between errors in a model can be computed by Durbin–Watson statistic. The value of DW statistic is between 0 and 4. The DW values below 2 illustrated positive autocorrelation and values above 2 demonstrated negative autocorrelation. If the DW value is typically around 2, this implies a good fit of the model [17]. According to results, the DW statistic (DW = 1.995) was determined to be very close to 2, indicating the goodness of fit of the model. The chi-square (χ^2) test is another statistical analyzed that shows a significant difference between the expected responses and the observed data. The calculated chi-square value ($\chi_{\text{cal}}^2 = 1.03$) was found to be less than the critical value ($\chi_{\alpha, (n-1)}^2 = \chi_{0.05, 26}^2 = \chi_{\text{tab}}^2 = 38.885$) suggesting that there was no significant difference between the observed and the expected responses. Overall, statistical analysis reflected that the experimental values fitted well with the predicted ones and the accuracy and general availability of the polynomial model were adequate for further optimization (Table 5).

3.3. Graphical interpretation of model by 3D response surface

The graphical inferences of the individual and cumulative effects of variables on response within the studied experimental range were presented through three-dimensional (3D) response surface. The 3D plots were generated by combinations of two test variables with the other two maintained at their respective optimum levels which are summarized in Fig. 3(a)–(f).

Fig. 3(a) illustrates the interactive effect of pH and adsorbent dosage on the response at constant initial dye concentration (20 mg L⁻¹) and temperature (32.5°C). It can be observed from this figure that the removal of dye from aqueous solution by modified SBA-15 increased as the pH of solution was changed from 3 to 10, which was also reflected in the obtained quadratic equation. The negative surface

charge of the MDA-SBA-15 is decreased with increasing pH resulting in strengthening of the electrostatic adsorption force between the adsorbent and MB molecules which caused enhancement of removal percentage of MB dye. Also the presence of excess H⁺ competing with the cationic dyes for adsorption sites in acidic solutions [26]. Moreover, Fig. 3(a) shows that *R*% increased with an increase in adsorbent dose. Fig. 3(b) presented the combined effect of pH and initial dye concentration on response while adsorbent dosage and temperature was held at central level. Maximum percentage removal of dye was obtained at maximum pH (10) and lower dye concentration (10 mg L⁻¹). The 3D response surface plot as a function of pH and temperature at constant adsorbent dose (2 g L⁻¹) and initial dye concentration (20 mg L⁻¹) are demonstrated in Fig. 3(c), which portended that the percentage removal decreased with an increase in the temperature, and confirming the exothermic nature of adsorption. At a temperature of 25°C, maximum percentage removal (94%) was obtained. The weakening of physical interactions between dyes and active adsorbent sites could be the significant contributor toward a decrease in percentage removal with an increase in the temperature [6]. As shown in Fig. 3(d), it could be observed that at constant pH (6.5) and temperature (32.5°C), the combined influence of adsorbent dosage and initial dye concentration had a significant effect on response. An increase in adsorbent dose from (0.5–3.5 g L⁻¹) and decrease in initial dye concentration from (30–10 mg L⁻¹) show an augmentation in percentage removal. This observation was a result of the concentration effect will inversely have an impact on its adsorption frequency which was an indicative of the adsorption constant because of the limited adsorption sites available for adsorption of dye.

It is transparent from Fig. 3(e) that the percentage removal has an increasing trend as adsorbent dose and temperature were decreased within the experimental range and optimum pH (6.5) and initial dye concentration (20 mg L⁻¹). From Fig. 3(f) it is also

Table 5
Detailed descriptive statistics of the regression analysis for quadratic model

Descriptive statistics	Calculation	Regression results
Durbin–Watson statistic	$DW = \frac{\sum_{i=2}^n (y_i - y_{i-1})^2}{\sum_{i=1}^n y_i^2}$	1.99
Mallow's C_p statistic	$C_p = \left(\frac{SS_E}{MSS_E} \right) + 2p - n$	5.0
(χ^2) test	$\chi_{\text{cal}}^2 = \sum_{i=1}^n (y_{\text{meas}} - y_{\text{per}})^2 / y_{\text{per}}$	1.03

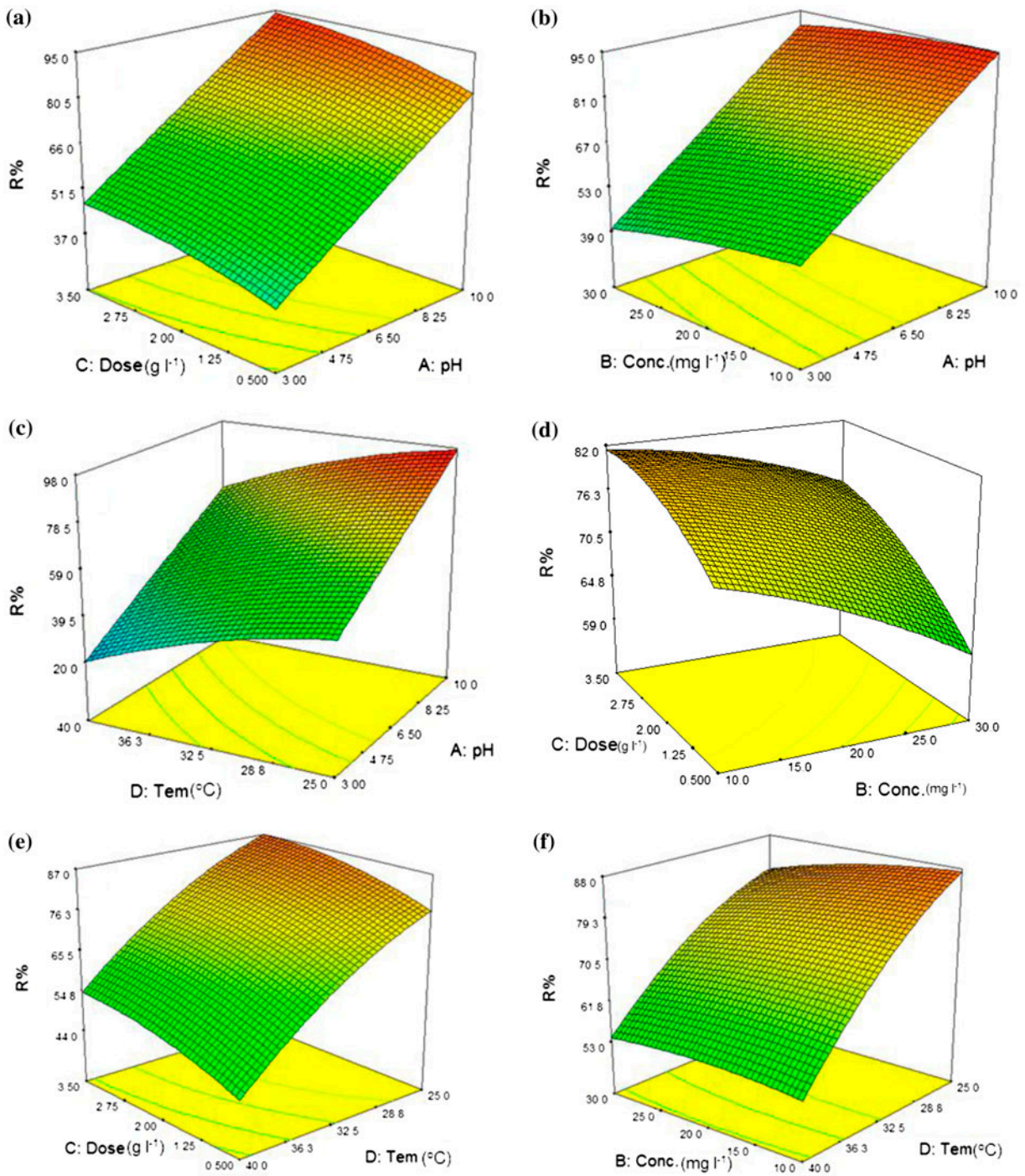


Fig. 3. 3D response surface and contour plots: interactive effects of (a) pH and adsorbent dose, (b) pH and initial dye concentration, (c) pH and temperature, (d) adsorbent dose and initial dye concentration, (e) adsorbent dose and temperature, and (f) initial dye concentration and temperature on adsorption efficiency of MB.

distinguished that under predefined conditions (constant pH and adsorbent dose at level 6.5 and 2 g L^{-1} , respectively), the percentage removal increased with diminishing initial dye concentration and temperature as previously.

3.4. Effects of model components and their interactions on MB adsorption efficiency

The significance of each coefficient was determined by Student's *t*-test and *p*-values, which are listed in Table 6. The *t*-value expresses the ratio of the estimated parameter effect to the estimated parameter standard deviation. Moreover, the *p*-values were applied as a tool to check the significance of the interactions between the coefficients of variables. Most significant of the corresponding parameter in the regression model was obtained by superlative magnitude of the *t*-value and smaller the *p*-value.

It can be seen from Table 6 that two first-order term coefficients (pH and temperature) were found more statistically significant than their respective quadratic and interaction term coefficients as was evident from their respective *t*-ratios and *p*-values. The most significant component of the regression model was found as the initial pH of solution (A) for the present application ($t = 98.9$, $p = 0.0001$). Among all model components, the four quadratic terms (A^2 , B^2 , C^2 , D^2)

demonstrated the lowest effect on the MB removal efficiency. A positive sign of the coefficients indicated a synergistic effect, while a negative sign denoted an antagonistic effect on percentage removal of MB. The linear terms (B and D), interaction terms (AD), and all second-order had a negative effect on the response. Hence, the response will decrease as these terms increase. The percentage contribution (PC) of each of the components was also calculated from the sum of squares obtained from the ANOVA (Table 6), as was similarly done by Singh et al. [18] for adsorption of crystal violet by magnetic nanocomposite. More contribution to the response correlates with higher PC value. In this way, it is clear from Table 6 that the greatest and most prominent components in determining the MB percentage removal are pH and temperature, which account for about 65.29 and 28.11%, respectively. The total percentage contributions (TPC) of the sum of squares for the first-order, quadratic, and interaction terms were calculated by the following equation, respectively.

$$TPC_i = \frac{\sum_{i=1}^n SS_i}{\sum_{i=1}^n \sum_{i=1}^n SS_i + SS_{ii} + SS_{ij}} \times 100 \quad (6)$$

$$TPC_{ii} = \frac{\sum_{i=1}^n SS_{ii}}{\sum_{i=1}^n \sum_{j=1}^n SS_i + SS_{ii} + SS_{ij}} \times 100 \quad (7)$$

Table 6
Multiple regression results and significance of the components for the quadratic model

Factor (coded)	Parameter	Coefficient	Effect	SE ^a	<i>t</i> ratio ^b	SS	PC (%) ^c
Intercept	β_0	59.5					
A-pH	β_a	23	46	0.465	98.92473	8,710	65.29
B-Conc.	β_b	-3.91	-7.82	0.465	-16.8172	253	1.9
C-Dose	β_c	5.46	10.92	0.465	23.48387	492	3.69
D-Tem	β_d	-15.1	-30.2	0.465	-64.9462	3,750	28.11
AB	β_{ab}	1.65	3.3	0.472	6.991525	43.6	0.33
AC	β_{ac}	0.55	1.1	0.472	2.330508	4.84	0.04
AD	β_{ad}	-0.1	-0.2	0.472	-0.42373	0.16	0
BC	β_{bc}	1.43	2.86	0.472	6.059322	32.5	0.24
BD	β_{bd}	1.77	3.54	0.472	7.5	50.4	0.38
CD	β_{cd}	0.175	0.35	0.472	0.741525	0.49	0
A^2	β_{A^2}	-0.26	-0.52	4.63	-0.11231	0.0113	0
B^2	β_{B^2}	-1.26	-2.52	4.63	-0.54428	0.264	0
C^2	β_{C^2}	-2.26	-4.52	4.63	-0.97624	0.85	0.01
D^2	β_{D^2}	-3.9	-7.8	4.62	-1.68831	2.54	0.02

^aStandard error.

^b*t* = effect/SE.

^cPC = SS/∑SS × 100.

$$\text{TPC}_{ij} = \frac{\sum_{i=1}^n \text{SS}_{ij}}{\sum_{i=1}^n \sum_{j=1}^n \text{SS}_i + \text{SS}_{ii} + \text{SS}_{ij}} \times 100 \quad (8)$$

where TPC_i , TPC_{ii} , and TPC_{ij} are the TPC of first-order, quadratic, and interaction terms, respectively. Similarly, SS_i , SS_{ii} , and SS_{ij} are the computed sum of squares for first-order, quadratic, and interaction terms, respectively (Table 6). As a result, the first-order terms exhibited the highest percentage, with a total contribution of 98.8%. The rest of the contribution from the quadratic and interaction terms was less than 2% considering insignificant for predicting the percentage removal of MB. Therefore, it can be concluded that the first-order independent variables have a more direct effect on the regression model than the other ones.

3.5. Optimization condition

The optimization of the variables condition was performed with main objective of obtaining maximum percentage removal toward MB dye as organic compounds. Design expert as a multiple response method was applied for optimization of any combination of four factors, namely initial solution pH, initial dye concentration, adsorbent dose, and temperature. The condition that was considered optimum selected from desirability function close to 1.0. According to the RSM optimization step, the desired goal for each operational condition was chosen “within the range”, while the response (percentage removal) was defined as “maximum” to achieve highest performance. On the basis of desirability score of 1.0, maximum removal efficiency (98%) was obtained at optimum conditions set as: pH 10, 3 g L⁻¹ of adsorbent dose and MB initial concentration of 10 mg L⁻¹ at 25 °C. The corresponding experimental value of the percentage removal was determined as 96.5, which is in good agreement with the optimum value predicted by the

model. Hence, the model was found to be useful to predict the response as well as to optimize the process conditions.

3.6. Adequacy test of the models

It is usually necessary to check the fitted model to ensure that it provides an adequate approximation to the real system. In order to validate the developed model (Eq. (5)), experiments were conducted for 5 new trials, consisting of combinations of experimental factors, which do not belong to the training data-set. Experimentally determined response factor values for each of the five set of process variables were then used along with the model predicted values to compute the R^2 , RMSEP, and RSEP values. The results of the selected combinations of variable factors, actual and predicted values of response are given in Table 7.

As seen in Table 7, MB adsorption determined for the validation batch experiments showed a wide variation ranging from 49.3 to 89.7%. Relatively low RMSEP (1.32), RSEP (2.2) and considerably high correlation (99%) between predicted and measured values suggested that the model was accurate and reliable in predicting the response variable for the validation data-set comprised of different combinations of the process variable. Noticeable difference between the predicted values of the constructed RSM and the observed data obtained from the additional experiments were also measured by a non-parametric Mann–Whitney U -test. The basic procedure of the Mann–Whitney U -test is to work with the ranked data. Two independent samples are first combined into one column, and then the values are ranked from smallest to largest (where 1 = smallest). Finally, they are broken down into their original samples, and the total rank scores (U) of each are summed up. On the basis of the test procedure, an expected score is first determined as follows:

Table 7

Values of natural independent variables and corresponding output and ranked data for the statistical model validation

Additional batch no.	Uncoded variables				Removal efficiency (%)		Ranked data for the Mann–Whitney U -test	
	pH of solution	Concentration of MB (mg L ⁻¹)	Adsorbent dose (g L ⁻¹)	Temperature (°C)	Observed (R%)	Predicted (R%)	Observed	Predicted
1	7.37	15.8	0.57	26	70.3	68.8	7	8
2	6.5	28	0.73	25.5	61.1	58.4	5	6
3	9	14.5	3.4	27	89.7	87.4	10	9
4	5.5	27.6	3.1	30	49.3	49	4	3

$$E(U) = \frac{n_u(N+1)}{2} \quad (9)$$

where $E(U)$ is the expectation of U , n_u is the sample size of the data-set being tested, and N is the total number of samples ($N = n_1 + n_2$). Thereafter, the Z score under the normal curve is calculated according to the following equation:

$$Z = U_{\max} - E(U) / \sqrt{\frac{n_1 n_2 (N+1)}{12}} \quad (10)$$

where U_{\max} is the maximum total rank score, and n_1 and n_2 are the sample sizes of the independent samples. For the present validation data the Z score was determined to be 1.04 according to Eqs. (9) and (10). Then, the two-tailed probability associated with the obtained Z score under the normal curve was obtained as $p = 0.87$, which was greater than the chosen α -level ($0.87 > 0.05$), since the alternative hypothesis was rejected in favor of the null hypothesis, indicating that there was no statistically significant difference between the measured data and the predicted response. In order to evaluate the relationship between the model predicted and the experimental responses, a parametric two-sample (unpaired) t -test was also performed following calculation of the pooled standard error as follows:

$$Se_p = \frac{(S_1 + S_2)}{2} \sqrt{\frac{1}{n_1} + \frac{1}{n_2}} \quad (11)$$

$$t_{\text{cal}} = Y_1^- - \frac{Y_2^-}{Se_p} \quad (12)$$

where Se_p is the pooled standard error, S_1 and S_2 are the standard deviations of the samples, n_1 and n_2 are the sample sizes of the independent samples, t_{cal} is the calculated t -statistic, and Y_1^- and Y_2^- are the mean values of the independent samples.

The value was compared with the critical t -value (t_{crit}) for the corresponding degrees of freedom ($df = n_1 + n_2 - 1$). The calculated t -value ($t_{\text{cal}} = 0.148$) was found to be less than the critical value of t ($t_{\text{crit}} = 2.36$), suggesting that there is no significant statistical difference between the two set of independent samples, as previously found in the Mann–Whitney test. Therefore, both the non-parametric Mann–Whitney test and the two-sample t -test with 95% certainty that the proposed quadratic model provided a satisfactory fit to the validation data-set.

3.7. Modeling of MB adsorption by MDA-SBA-15

3.7.1. Isotherm

Equilibrium adsorption isotherms are of fundamental importance in the design of adsorption systems for practical applications, since it can provide information about the surface properties of adsorbent and nature of the adsorption phenomenon. In order to interpret the specific relationship between the concentration of adsorbate and its extent of adsorption onto the adsorbent surface at a constant temperature, three isotherm models, Langmuir, Freundlich, and Temkin were constructed using experimental equilibrium data obtained from the study of MB adsorption on MDA-SBA-15 at initial dye concentrations of 5–35 mg L⁻¹ at pH 10.

The Langmuir isotherm theory depicts that adsorption takes place at the specific homogeneous sites within the adsorbent with no interaction between the adsorbent molecules. In addition, the adsorbent has a finite capacity for the adsorbent, where all sorption sites are identical and energetically equivalent. The Langmuir isotherm can be represented by following equation [27]:

$$q_e = \frac{q_m K_L C_e}{1 + K_L C_e} \quad (13)$$

The Langmuir parameters q_e (mg g⁻¹) is the amount of dye adsorbed by the MDA-SBA-15 at equilibrium, C_e (mg L⁻¹) is the equilibrium dye concentration, K_L (L mg⁻¹) is the Langmuir constant and q_m (mg g⁻¹) represents maximum monolayer capacity of adsorbent.

Unlike the Langmuir isotherm, the Freundlich isotherm is an empirical equation which is derived by assuming a heterogeneous surface with a non-uniform distribution of the heat of adsorption over the surface. The Freundlich isotherm can be expressed by Eq. (14) [28]:

$$q_e = K_F C_e^{1/n_F} \quad (14)$$

K_F is a constant relating to the adsorption capacity, and $1/n_F$ is an empirical parameter relating to the adsorption intensity. $1/n_F$ with favorable range between (0–1), irreversible (0) and unfavorable (>1), is a measure of adsorption intensity and surface heterogeneity [29].

The Temkin isotherm [30] has been applied in the following form to evaluate heat of adsorption of adsorbate molecules with the extent of coverage over the surface of adsorbent particles. It assumes that the fall of adsorption heat is linear rather than logarithmic.

$$q_e = \frac{RT}{b_T} \ln A_T + \frac{RT}{b_T} \ln C_e \tag{15}$$

where $B = R_T/b_T$, T is the absolute temperature (K) and R is the ideal gas constant ($8.314 \text{ J (mol K)}^{-1}$). The constant b_T and A_T , which is related to the heat of adsorption and equilibrium binding constant corresponding to the maximum binding energy, are determined from the slope and intercepts of the plots obtained by plotting q_e vs. $\ln C_e$. The graphical presentation of relationship between the adsorption experimental data of MB on the surface of MDA-SBA-15 and theoretical data by applying Langmuir, Freundlich, and Temkin isotherm is expressed in Fig. 4(a) and (b). The data in Table 8 present the isotherm constants along with associated correlation coefficients (R^2). They reveal that all R^2 values are greater than 0.97, suggesting the adsorption process of MB onto MDA-SBA-15 could be well described by multifarious isotherms. However, the Langmuir model seemed to agree well with the experimental data considering that obtained linear regression coefficients are greater than other isotherms. Furthermore, the essential characteristic of the Langmuir isotherm can be expressed in terms of a dimensionless equilibrium parameter, the separation factor (R_L), which used in the following equation, $R_L = 1/(1 + K_L C_0)$. The value of parameter R_L indicates the nature of the adsorption process which irreversible ($R_L = 0$), favorable ($0 < R_L < 1$), linear ($R_L = 1$), or unfavorable ($R_L > 1$). The value of R_L for the present system comes out to be 0.1, communicating the favorable adsorption of dye MB onto MDA-SBA-15. The values of Freundlich constant $1/n_F$ is between 0 and 1.0 which also indicated that adsorption of MB under the studied condition are suitable. Moreover, the variation of the adsorption energy b_T obtained from the Temkin equation was positive, which indicated that the adsorption reaction was exothermic [31]. Thus, the applicability of the Langmuir model suggests that adsorption occurs at specific homogeneous sites within the adsorbent, and once a dye molecule resides at a site, no further adsorption takes place at that site. A similar phenomenon has been observed in the adsorption of MB onto SBA-15 [32].

3.7.2. Kinetic

Adsorption kinetics assists in evaluating the rate and mechanism of mass transfer of adsorbate from liquid phase to solid adsorbent surface. Several kinetics models are needed to examine the mechanism of the

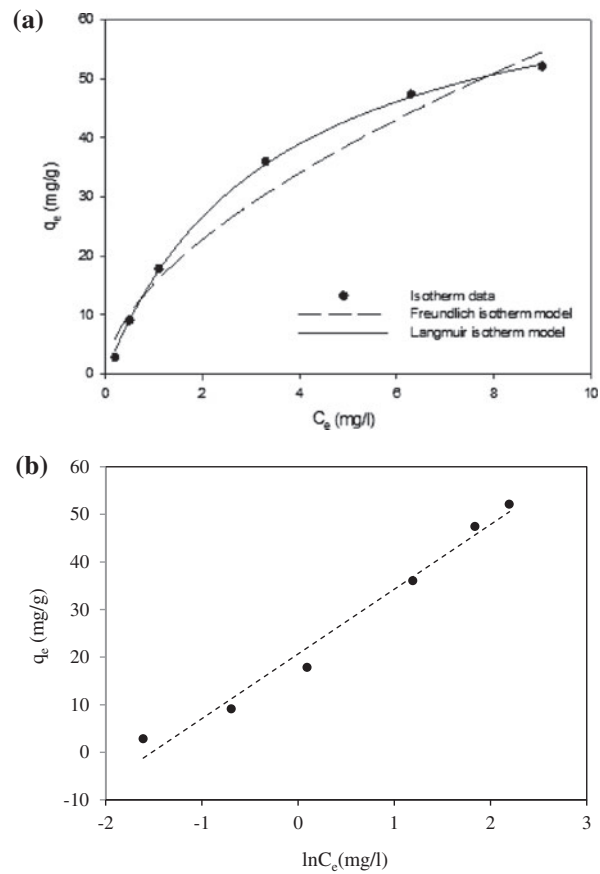


Fig. 4. Langmuir and Freundlich (a) and Temkin (b) isotherm fits for MB adsorption onto MDA-SBA-15 (initial pH, 10; adsorbent dose, 0.5 g l^{-1}).

Table 8
Adsorption isotherm constants of the three isotherm models for MB adsorption on MDA-SBA-15

Isotherms	Parameters	
Langmuir	$K_L \text{ (L mg}^{-1}\text{)}$	0.29
	R_L	0.10
	R^2	0.999
Freundlich	$K_F \text{ ((mg g}^{-1}\text{)(L mg}^{-1}\text{))}$	15.23
	n_F	1.72
	R^2	0.993
Temkin	$A_T \text{ (L mg}^{-1}\text{)}$	20.82
	b_T	13.68
	R^2	0.979

solute sorption onto a sorbent. In this work, pseudo-first-order, pseudo-second-order and Weber-Morris (intra-particle diffusion) models [26] were fitted to the experimental data for the determination of potential

rate-controlling steps of the MB adsorption kinetics (Table 9).

Linear form of the pseudo-first-order model was expressed as:

$$\log(q_e - q_t) = \log(q_e) - \frac{k_1}{2.303}t \quad (16)$$

where q_e and q_t are the adsorption capacities (mg g^{-1}) at equilibrium and at time t , respectively, and k_1 (min^{-1}) is the equilibrium rate constant of pseudo-first-order equation. The slope and intercept of the graph of $\log(q_e - q_t)$ vs. t show the value of constants k_1 and q_e (Fig. 5(a)). The pseudo-second-order equation of McKay and Ho can be represented as:

$$\frac{t}{q_t} = \frac{1}{k_2 q_e^2} + \frac{t}{q_e} \quad (17)$$

where k_2 ($\text{g}(\text{mg min})^{-1}$) is the rate constant of second-order adsorption. Analysis of the experimental data with the pseudo-second-order kinetic model provided linear plots of t/q_t vs. t (Fig. 5(b)). From both comparison of experimental and theoretical calculation on an adsorbent and linear regression coefficient values, it could be indicated the inapplicability of the pseudo-first-order models for analyzing the adsorption kinetics of MB by MDA-SBA-15.

The fittings of the adsorption data with the pseudo-second-order kinetic model is presented in Fig. 5(b). In contrast to the kinetic models, the pseudo-second-order model fitted the experimental data well, with exceptionally high correlation coefficients ($R^2 = 1$). The values of q_e calculated using pseudo-second-order model was similar to the experimental values (58.8 mg g^{-1}), implying that the MB adsorption

Table 9

Kinetic constants of pseudo-first-order and pseudo-second-order and intra-particle diffusion kinetic models

Kinetic models	Model parameter	
Pseudo-first-order	q_e (mg g^{-1})	2.169
	k_1 (1 min^{-1})	0.76
	R^2	0.91
Pseudo-second-order	q_e (mg g^{-1})	58.13
	k_2 ($\text{g}(\text{mg min})^{-1}$)	0.99
	R^2	1.0
Intra-particle diffusion	k_{id1} ($\text{mg}(\text{gmin}^{0.5})^{-1}$)	0.473
	k_{id2} ($\text{mg}(\text{gmin}^{0.5})^{-1}$)	0.289
	k_{id3} ($\text{mg}(\text{gmin}^{0.5})^{-1}$)	0.004

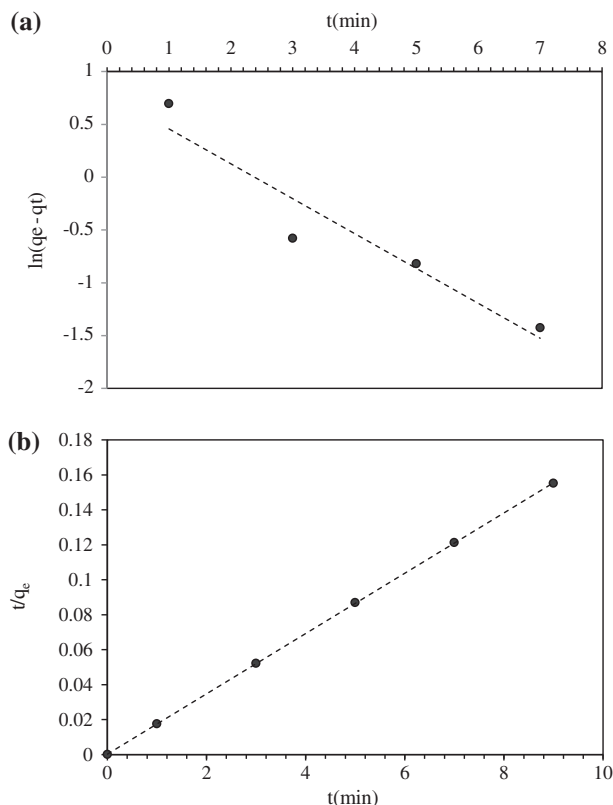


Fig. 5. Pseudo-first-order and (a), pseudo-second-order (b), intra-particle diffusion (c) kinetics for sorption of MB onto MDA-SBA-15.

can be described more appropriately by the pseudo-second-order model. It also assumes that the rate-controlling step of the adsorption process of MB on MDA-SBA-15 is governed by chemisorption [26].

Although the pseudo-second-order equation was found to fit the experimental data very well, the results obtained from this model are not sufficient to predict the diffusion mechanism [33]. Therefore, the kinetic behavior of the adsorption process was further analyzed using the intra-particle diffusion model according to the Eq. (18). External diffusion and internal diffusion (or intra-particle diffusion), which can be investigated by plotting the q_t against $t^{0.5}$, are the two stages for the adsorption process on a porous adsorbent [34].

The slowest step, which might be either external diffusion or internal diffusion, would obviously be the overall rate-controlling step of the adsorption process.

$$q_t = K_{id}t^{0.5} \quad (18)$$

where k_{id} ($\text{mg g}^{-1} \text{ min}^{-0.5}$) is the intra-particle diffusion constant. If the straight line passes through

the origin, then intra-particle diffusion is the rate-controlling step. Otherwise, the adsorption process may involve some other mechanisms along with the intra-particle diffusion [35]. Fig. 5(c) presents the fitting of the experimental data with the intra-particle diffusion model. It can be clearly observed from this figure that plots of q_t vs. $t^{0.5}$ are not linear over the whole time range and can be separated into three linear regions. The multilinearity of the plots confirms the involvement of multistage adsorption process [36]. The initial linear portion of the plot is due to external mass transfer, which allows the adsorbate molecules to be transported to the external surface of the MDA-SBA-15 through film diffusion. The solute molecules entered the interior of the adsorbent by intra-particle diffusion through pores, as reflected by the second linear portion of the plot. The third portion of plot represents the equilibrium stage which the intra-particle diffusion started to slow and become stagnant as the adsorbate molecules occupied all of the active sites of the adsorbent and the maximum adsorption was attained [35–37]. In addition, the slope of the linear portion implies the diffusion rate decreased with an increase in the contact time (from $k_{id,1}$ to $k_{id,3}$), which was ascribed to a decreasing free path of the molecules in the pore of the adsorbents and film diffusion step was an important step for the adsorption of MB onto the MDA-SBA-15. A similar phenomenon was observed in the adsorption of dye by various adsorbent [26,38].

3.7.3. Thermodynamic

Temperature variation of 298, 301.5, 305, 309, and 318 ± 1 K were used in order to study the effect of temperature on the adsorption of MB by MDA-SBA-15. The adsorption capacity of the modified SBA-15 was found to be reduced with raising temperature from 298 to 318 K, thereby demonstrating the exothermic nature of the adsorption.

The values of the thermodynamic parameters such as the Gibbs' free energy (ΔG), the standard enthalpy change (ΔH), and the standard entropy change (ΔS), which help to deliberate the nature of dye adsorption and heat change for adsorption reaction, were investigated using the following equation:

$$\Delta G = -RT \ln K \quad (19)$$

$$\ln K = \frac{\Delta S}{R} - \Delta H/RT \quad (20)$$

where K is the distribution coefficient expressed as $K = q_e C_e^{-1}$, R is the universal gas constant (8.314 J

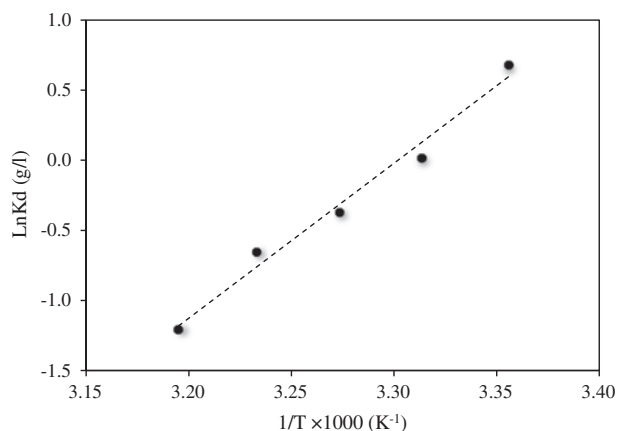


Fig. 6. Vant Hoff plot for adsorption of MB onto MDA-SBA-15.

(K mol⁻¹), and T is the absolute temperature (K). A linear plot of $\ln K$ vs. $1/T$ (K⁻¹) is constructed to generate ΔH and ΔS from the intercept and slope (Fig. 6).

The values of ΔG obtained from Eq. (19) are (-1.47, -0.32, 0.65, 1.96, 3.08 kJ mol⁻¹) for MB adsorption on MDA-SBA-15 in temperatures range. The negative value of ΔG verified the thermodynamic feasibility and spontaneity of the adsorption process. The favorability of MB adsorption onto modified SBA-15 at low temperature was also revealed by the shifting of ΔG to negative values with decreasing temperature. The negative value of change in enthalpy ΔH (-91.85 kJ mol⁻¹) shows the exothermic nature of adsorption processes, which is in accordance with the results obtained from the adsorption equilibrium isotherms. On the other hand, negative value of change in entropy ΔS (-0.304 kJ mol⁻¹) reflects that disordering at the solid-liquid interface decreased during dye adsorption and that no significant changes occurred in the internal structure of the adsorbents upon adsorption, respectively. This is similar to the result of adsorption MB by mesoporous silicas [13,32,39].

4. Conclusion

Melamine-based dendrimer amine was covalently tethered at the surface of mesostructure SBA-15 with the aim of testing their MB adsorption efficiency. From XRD, FT-IR, SEM, and N₂ adsorption-desorption data, the successful functionalization of SBA-15 mesoporous silica with MDA was assessed. The dependency of absorption process on pH, initial dye concentration of solution, adsorbent dosage, and temperature was studied using RSM, which provided an effective means to

help in understanding the relative or interactive effects of variables. According to the proposed quadratic model, pH and temperature terms were determined to be the most significant components because of their contribution of about 65.29 and 28.11, respectively. In addition, the experimental data matched well with the predicted values derived from the quadratic model, with a correlation coefficient of 0.9959, CV = 3.44%, $C_p = 5$, and DW = 1.99. The statistical results showed that the first-order terms contributed about 98.8% to the MB adsorption efficiency than their respective quadratic effects, indicating that the selected variables had a direct relationship on the response. It was observed that the removal efficiency of MDA-SBA-15, as obtained through optimization of process variables by RSM (98% at pH 9, adsorbent dose 3 g L^{-1} , adsorbate concentration 10 mg L^{-1} , and temperature 25°C), was close to the experimentally determined value (96.5%). Further the prediction capability of the quadratic model was verified by additional batch experiments conducted in the experimental scale. The validation results clearly confirmed with 95% certainty. The adsorption process agreed reasonably well with the Langmuir isotherm which suggested that MB adsorption onto MDA-SBA-15 was a homogeneous adsorption. The adsorption process was well described by the pseudo-second-order kinetic model, and intraparticle diffusion involved in the adsorption process but was not the only rate-controlling step. Thermodynamics analysis revealed maximum adsorption was achieved at room temperature that slightly decreased with an increase in temperature, reflecting exothermic nature of adsorption and spontaneous. It was also confirmed by Temkin constant. In conclusion, the outcomes from this investigation support the view that MDA-SBA-15 is an effective adsorbent and the CCD experimental design combining with RSM would be an effective tool for mathematical modeling and optimization of the MB adsorption process.

Acknowledgments

Authors wish to thank the Iranian Nano Technology Initiative Council for financial support. The authors also wish to thank Shahid Beheshti University for considerable laboratory support.

References

- [1] M.Ş. Tanyildizi, Modeling of adsorption isotherms and kinetics of reactive dye from aqueous solution by peanut hull, *Chem. Eng. J.* 168 (2011) 1234–1240.
- [2] K. Sinha, S. Chowdhury, P.D. Saha, S. Datta, Modeling of microwave-assisted extraction of natural dye from seeds of *Bixa orellana* (Annatto) using response surface methodology (RSM) and artificial neural network (ANN), *Ind Crops and Prod.* 41 (2013) 165–171.
- [3] P. Monash, G. Pugazhenth, Investigation of equilibrium and kinetic parameters of methylene blue adsorption onto MCM-41, *Korean J. Chem. Eng.* 27 (2010) 1184–1191.
- [4] L.W. Low, T.T. Teng, A.F. Alkarkhi, A. Ahmad, N. Morad, Optimization of the adsorption conditions for the decolorization and COD reduction of methylene blue aqueous solution using low-cost adsorbent, *Water, Air, Soil Pollut.* 214 (2011) 185–195.
- [5] M. Rafatullah, O. Sulaiman, R. Hashim, A. Ahmad, Adsorption of methylene blue on low-cost adsorbents: A review, *J. Hazard. Mater.* 177 (2010) 70–80.
- [6] S. Nayab, A. Farrukh, Z. Oluz, E. Tuncel, S.R. Tariq, H.u. Rahman, K. Kirchhoff, H. Duran, B. Yameen, Design and fabrication of branched polyamine functionalized mesoporous silica: An efficient adsorbent for water remediation, *ACS Appl. Mater. Interfaces* 6 (2014) 4408–4417.
- [7] M. Roosta, M. Ghaedi, A. Daneshfar, R. Sahraei, A. Asghari, Optimization of the ultrasonic assisted removal of methylene blue by gold nanoparticles loaded on activated carbon using experimental design methodology, *Ultrason. Sonochem.* 21 (2014) 242–252.
- [8] J.B. Joo, J. Park, J. Yi, Preparation of polyelectrolyte-functionalized mesoporous silicas for the selective adsorption of anionic dye in an aqueous solution, *J. Hazard. Mater.* 168 (2009) 102–107.
- [9] A. Karim, A. Jalil, S. Triwahyono, N. Kamarudin, N. Salleh, Amino modified mesostructured silica nanoparticles for efficient adsorption of methylene blue, *J. Colloid Interface Sci.* 386 (2012) 307–314.
- [10] C.H. Huang, K.P. Chang, H.D. Ou, Y.C. Chiang, E.E. Chang, C.F. Wang, Characterization and application of Ti-containing mesoporous silica for dye removal with synergistic effect of coupled adsorption and photocatalytic oxidation, *J. Hazard. Mater.* 186 (2011) 1174–1182.
- [11] E. Da'na, A. Sayari, Adsorption of copper on amine-functionalized SBA-15 prepared by co-condensation: Equilibrium properties, *Chem. Eng. J.* 166 (2011) 445–453.
- [12] T. Kang, Y. Park, K. Choi, J.S. Lee, J. Yi, Ordered mesoporous silica (SBA-15) derivatized with imidazole-containing functionalities as a selective adsorbent of precious metal ions, *J. Mater. Chem.* 14 (2004) 1043–1049.
- [13] S. Eftekhari, A. Habibi-Yangjeh, S. Sohrabnezhad, Application of AIMCM-41 for competitive adsorption of methylene blue and rhodamine B: Thermodynamic and kinetic studies, *J. Hazard. Mater.* 178 (2010) 349–355.
- [14] A. Shahbazi, H. Younesi, A. Badii, Functionalized SBA-15 mesoporous silica by melamine-based dendrimer amines for adsorptive characteristics of Pb(II), Cu(II) and Cd(II) heavy metal ions in batch and fixed bed column, *Chem. Eng. J.* 168 (2011) 505–518.
- [15] D. Zhao, J. Feng, Q. Huo, N. Melosh, G.H. Fredrickson, B.F. Chmelka, G.D. Stucky, Triblock copolymer syntheses of mesoporous silica with periodic 50 to 300 angstrom pores, *Science* 279 (1998) 548–552.

- [16] S. Chowdhury, P.D. Saha, Scale-up of a dye adsorption process using chemically modified rice husk: optimization using response surface methodology, *Desalin. Water Treat.* 37 (2012) 331–336.
- [17] K. Yetilmezsoy, S. Demirel, R.J. Vanderbei, Response surface modeling of Pb(II) removal from aqueous solution by *Pistacia vera* L: Box-Behnken experimental design, *J. Hazard. Mater.* 171 (2009) 551–562.
- [18] K.P. Singh, S. Gupta, A.K. Singh, S. Sinha, Optimizing adsorption of crystal violet dye from water by magnetic nanocomposite using response surface modeling approach, *J. Hazard. Mater.* 186 (2011) 1462–1473.
- [19] A. Shahbazi, H. Younesi, A. Badiei, Batch and fixed-bed column adsorption of Cu(II), Pb(II) and Cd (II) from aqueous solution onto functionalised SBA-15 mesoporous silica, *Can. J. Chem. Eng.* 91 (2013) 739–750.
- [20] B. Li, R. Yan, L. Wang, Y. Diao, Z. Li, S. Zhang, SBA-15 supported cesium catalyst for methyl methacrylate synthesis via condensation of methyl propionate with formaldehyde, *Ind. Eng. Chem. Res.* 53 (2014) 1386–1394.
- [21] S. Badoga, A.K. Dalai, J. Adjaye, Y. Hu, Combined effects of EDTA and heteroatoms (Ti, Zr, and Al) on catalytic activity of SBA-15 supported NiMo catalyst for hydrotreating of heavy gas oil, *Ind. Eng. Chem. Res.* 53 (2014) 2137–2156.
- [22] Z. Liang, B. Fadhel, C.J. Schneider, A.L. Chaffee, Stepwise growth of melamine-based dendrimers into mesopores and their CO₂ adsorption properties, *Microporous Mesoporous Mater.* 111 (2008) 536–543.
- [23] A.L. Cazetta, O.P. Junior, A.M. Vargas, A.P. da Silva, X. Zou, T. Asefa, V.C. Almeida, Thermal regeneration study of high surface area activated carbon obtained from coconut shell: Characterization and application of response surface methodology, *J. Anal. Appl. Pyrolysis.* 101 (2013) 53–60.
- [24] M. Ghaedi, M.D. Ghazanfarkhani, S. Khodadoust, N. Sohrabi, M. Oftade, Acceleration of methylene blue adsorption onto activated carbon prepared from dross licorice by ultrasonic: Equilibrium, kinetic and thermodynamic studies, *J. Ind. Eng. Chem.* 20 (2014) 2548–2560.
- [25] P. Dawson, R. Martinez-Dawson, Using response surface analysis to optimize the quality of ultrapasteurized liquid whole egg, *Poultry Sci.* 77 (1998) 468–474.
- [26] L. Chen, B. Bai, Equilibrium, kinetic, thermodynamic, and in situ Regeneration studies about methylene blue adsorption by the raspberry-like TiO₂@yeast Microspheres, *Ind. Eng. Chem. Res.* 52 (2013) 15568–15577.
- [27] T.W. Weber, R.K. Chakravorti, Pore and solid diffusion models for fixed-bed adsorbers, *AIChE J.* 20 (1974) 228–238.
- [28] H. Freundlich, Over the adsorption in solution, *J. Phys. Chem.* 57 (1906) 1100–1107.
- [29] L. Eskandarian, M. Arami, E. Pajootan, Evaluation of Adsorption characteristics of multiwalled carbon nanotubes modified by a poly(propylene imine) dendrimer in single and multiple dye solutions: Isotherms, kinetics, and thermodynamics, *J. Chem. Eng. Data* 59 (2014) 444–454.
- [30] K. Hall, L. Eagleton, A. Acrivos, T. Vermeulen, Pore- and solid-diffusion kinetics in fixed-bed adsorption under constant-pattern conditions, *Ind. Eng. Chem. Fundam.* 5 (1966) 212–223.
- [31] O. Hamdaoui, Batch study of liquid-phase adsorption of methylene blue using cedar sawdust and crushed brick, *J. Hazard. Mater.* 135 (2006) 264–273.
- [32] C.H. Huang, K.P. Chang, H.D. Ou, Y.C. Chiang, C.F. Wang, Adsorption of cationic dyes onto mesoporous silica, *Microporous Mesoporous Mater.* 141 (2011) 102–109.
- [33] M.S. Sajab, C.H. Chia, S. Zakaria, S.M. Jani, M.K. Ayob, K.L. Chee, P.S. Khiew, W.S. Chiu, Citric acid modified kenaf core fibres for removal of methylene blue from aqueous solution, *Bioresour. Technol.* 102 (2011) 7237–7243.
- [34] S. Kaur, S. Rani, R. Mahajan, M. Asif, V.K. Gupta, Synthesis and adsorption properties of mesoporous material for the removal of dye safranin: Kinetics, equilibrium, and thermodynamics, *J. Ind. Eng. Chem.* 22 (2015) 19–27, doi: 10.1016/j.jiec.2014.06.019.
- [35] S. Haider, F.F. Binagag, A. Haider, A. Mahmood, N. Shah, W.A. Al-Masry, S.U.-D. Khan, S.M. Ramay, Adsorption kinetic and isotherm of methylene blue, safranin T and rhodamine B onto electrospun ethylenediamine-grafted-polyacrylonitrile nanofibers membrane, *Desalin. Water Treat.* 1 (2014) 1–11.
- [36] J. Fu, Z. Chen, M. Wang, S. Liu, J. Zhang, J. Zhang, R. Han, Q. Xu, Adsorption of methylene blue by a high-efficiency adsorbent (polydopamine microspheres): Kinetics, isotherm, thermodynamics and mechanism analysis, *Chem. Eng. J.* 259 (2015) 53–61.
- [37] A. Badiei, A. Mirahsani, A. Shahbazi, H. Younesi, M. Alizadeh, Adsorptive removal of toxic dye from aqueous solution and real industrial effluent by tris(2-aminoethyl) amine functionalized nanoporous silica, *Environ. Prog. Sustainable Energy* 33 (2014) 1242–1250.
- [38] S. Zeng, S. Duan, R. Tang, L. Li, C. Liu, D. Sun, Magnetically separable Ni_{0.6}Fe_{2.4}O₄ nanoparticles as an effective adsorbent for dye removal: Synthesis and study on the kinetic and thermodynamic behaviors for dye adsorption, *Chem. Eng. J.* 258 (2014) 218–228.
- [39] P.V. Messina, P.C. Schulz, Adsorption of reactive dyes on titania-silica mesoporous materials, *J. Colloid Interface Sci.* 299 (2006) 305–320.